Presentation at 51st AIAA Aerospace Sciences Meeting, 7-10 January 2013, Dallas, Texas

Transition Within a Hypervelocity Boundary Layer on a 5-Degree Half-Angle Cone in Air/CO_2 Mixtures

Joseph S. Jewell*
California Institute of Technology, Pasadena, CA, 91125

Ross M. Wagnild†
Sandia National Laboratories, Albuquerque, NM, 87185

Ivett A. Leyva‡
Air Force Research Laboratory, Edwards AFB, CA, 93536

Graham V. Candler§
University of Minnesota, Minneapolis, MN, 55455

Joseph E. Shepherd¶
California Institute of Technology, Pasadena, CA, 91125

Laminar to turbulent transition on a smooth 5-degree half angle cone at zero angle of attack is investigated computationally and experimentally in hypervelocity flows of air, carbon dioxide, and a mixture of 50% air and carbon dioxide by mass. Transition N factors above 10 are observed for air flows. At comparable reservoir enthalpy and pressure, flows containing carbon dioxide are found to transition up to 30% further downstream on the cone than flows in pure air in terms of x-displacement, and up to 38% and 140%, respectively, in terms of the Reynolds numbers calculated at edge and reference conditions.

Nomenclature

f	frequency
h	enthalpy
M	Mach number
P	pressure
Pr	Prandtl number
R	specific gas constant
T	temperature
u	velocity
w	mass fraction
x	displacement from the tip
γ	ratio of specific heats
δ	boundary layer thickness
Θ	characteristic vibrational temperature
μ	dynamic viscosity
ρ	density
τ	vibrational relaxation time

*Ph.D. Candidate, GALCIT, MC 205-45, Caltech. AIAA Student Member.
†Senior Member, Technical Staff, Sandia National Laboratories. AIAA Member.
‡Sr. Aerospace Engineer, Air Force Research Laboratory. AIAA Associate Fellow.
§Professor, University of Minnesota. AIAA Fellow.
¶Professor, GALCIT, MC 105-50, Caltech. AIAA Senior Member.

Subscript

e	condition at the boundary layer edge
res	condition in the reservoir
tr	condition at the location of transition
w	condition at the wall

Superscript

$*$	condition at Dorrance reference temperature

I. Introduction

In hypervelocity flow over cold, slender bodies, the most significant instability mechanism is the so-called second or Mack mode. These flows are characteristic of high-enthalpy facilities like the T5 shock tunnel at Caltech. A second mode disturbance depends on the amplication of acoustic waves trapped in the boundary layer, as described by Mack.[1] Another potential disturbance is the first mode, which is the high speed equivalent of the viscous Tollmien–Schlichting instability.[2] However, at high Mach number (> 4) and for cold walls, the first mode is damped and higher modes are amplified, so that the second mode would be expected to be the only mechanism of linear instability leading to transition for a slender cone at zero angle of attack.

Parametric studies in air and CO_2 in the T5 hypervelocity reflected shock tunnel by Germain[3] and Adam[4] on a smooth 5-degree half angle cones at zero angle of attack showed an increase in the reference Reynolds number Re* (see Equation 6 on page 8) at the point of transition as reservoir enthalpy h_{res} increased. Germain and Adam also observed that flows of CO_2 transitioned at higher values of Re* than flows of air for the same h_{res} and P_{res}. Johnson et al.[5] studied this effect with a linear stability analysis focused on the chemical composition of the flow, and found an increase in transition Reynolds number with freestream total enthalpy, and further found the increase to be greater for gases with lower dissociation energies and multiple vibrational modes, such as CO_2. In fact, with the assumption of a transition N factor of 10 that was made at the time, none of the CO_2 cases computed by Johnson et al. predicted transition at all. These effects led Fujii and Hornung[6] to further investigate their hypothesis that the delay in transition was due to the damping of acoustic disturbances in non-equilibrium relaxing gases by vibrational absorption. Fujii and Hornung estimated the most strongly amplified frequencies for representative T5 conditions and found that these agreed well with the frequencies most effectively damped by non-equilibrium CO_2. This suggests that the suppression of the second mode through the absorption of energy from acoustic disturbances through vibrational relaxation is the dominant effect in delaying transition for high-enthalpy carbon dioxide flows.

Numerous studies have been made on inhibiting the second mode, and therefore preventing or delaying transition through the suppression of acoustic disturbances within the boundary layer; see Fedorov et al.[7] and Rasheed[8] for work focused on absorbing acoustic energy using porous walls. Another approach to suppression of the pressure waves that lead to transition centers around altering the chemical composition within the boundary layer to include species capable of absorbing acoustic energy at the appropriate frequencies. Efforts in this area to date have included preliminary experimental work on mixed freestream flows, e.g. Leyva et al.,[9] computations, e.g. Wagnild et al.,[10,11] and experiments with direct injection of absorptive gases into the boundary layer, e.g. Jewell et al.[12] The present aim is to confirm and extend these studies both computationally and experimentally by considering transition within a hypervelocity boundary layer on a 5-degree half-angle cone in freestream mixtures of air and carbon dioxide.

II. Background

By assuming that the boundary layer acts as an acoustic waveguide for disturbances (see Fedorov[13] for a schematic illustration of this effect), the frequency of the most strongly-amplified second-mode disturbances in the boundary layer may be estimated as Equation (1), as shown in Stetson.[14]

$$f \approx 0.8 \frac{u_e}{2\delta} \tag{1}$$

Here δ is the boundary layer thickness and u_e is the velocity at the boundary layer edge. For a typical T5 condition in air, with enthalpy of 10 MJ/kg and reservoir pressure of 50 MPa, the boundary layer thickness is on the order of 1.5 mm and the edge velocity is 4000 m/s. This indicates that the most

strongly amplified frequencies are in the 1 MHz range. This is broadly consistent with the results of Fujii and Hornung.[6] Kinsler et al.[15] provide a good general description of the mechanisms of attenuation of sound waves in fluids due to molecular exchanges of energy within the medium. The relevant exchange of energy for carbon dioxide in the boundary layer of a thin cone at T5-like conditions is the conversion of molecular kinetic energy (e.g. from compression due to acoustic waves) into internal vibrational energy. In real gases, molecular vibrational relaxation is a non-equilibrium process, and therefore irreversible. This absorption process has a characteristic relaxation time. The problem of sound propagation, absorption, and dispersion in a dissociating gas has been treated from slightly different perspectives by Clarke and McChesney,[16] Zeldovich and Raizer,[17] and Kinsler et al.[15] However, in non-equilibrium flows when the acoustic characteristic time scale and relaxation time scale are similar, some finite time is required for molecular collisions to achieve a new density under an acoustic pressure disturbance. This results in a limit cycle, as the density changes lag the pressure changes. The area encompassed by the limit cycle's trajectory is related to energy absorbed by relaxation. Energy absorbed in this way is transformed into heat and does not contribute to the growth of acoustic waves.[9] Carbon dioxide, a linear molecule, has four normal vibrational modes. The first two, which correspond to transverse bending, are equal to each other, and have characteristic vibrational temperatures $\Theta_1 = \Theta_2 = 959.66$ K. The third mode, corresponding to symmetric longitudinal stretching, has $\Theta_3 = 1918.7$ K, and the fourth mode, corresponding to asymmetric longitudinal stretching, has $\Theta_4 = 3382.1$ K. Camac[18] showed that the four vibrational modes for carbon dioxide all relax at the same rate, and proposed a simplified formula, Equation (2), to calculate vibrational relaxation time, which was reproduced in Fujii and Hornung.[6]

$$\ln\left(A_4 \tau_{CO_2} P\right) = A_5 T^{-1/3} \tag{2}$$

Here A_4 and A_5 are constants given by Camac for carbon dioxide as $A_4 = 4.8488\times10^2$ Pa$^{-1}s^{-1}$ and $A_5 = 36.5$ K$^{1/3}$. Using the constants suggested by Camac, with $P = 35$kPa and $T = 1500$ K, which are consistent with a typical T5 condition with enthalpy 10 MJ/kg and stagnation pressure 50 MPa, we find vibrational relaxation time $= 1.43\times10^{-6}$ s, which indicates that frequencies around 700 KHz should be most strongly absorbed at these conditions. This is, again, broadly similar to the results of Fujii and Hornung,[6] who computed curves at 1000 K and 2000 K with peaks bracketing 700 kHz.

Thus, in a flow of gas that absorbs energy most efficiently at frequencies similar to the most strongly amplified frequencies implied by the geometry of the boundary layer, laminar to turbulent transition is expected to be delayed. Using computations, we show that the flow of carbon dioxide/air mixtures over a slender cone at T5 conditions allows for such a match in frequencies. We then perform a series of experiments to confirm this effect.

III. Experimental Model

The facility used in all experiments for the current study is the T5 hypervelocity reflected shock tunnel; see Hornung[19] and Hornung and Belanger.[20] The model is a smooth 5-degree half-angle aluminum cone similar to that used in a number of previous experimental studies in T5, 1 m in length, and is composed of three sections: a sharp tip (radius ∼0.2 mm) fabricated of molybdenum, an interchangeable mid-section which may contain a porous gas-injector section (in the present experiments this section is a smooth, solid piece of plastic), and the main body, which is instrumented with a total of 80 thermocouples evenly spaced at 20 lengthwise locations beginning at 221 mm from the tip of the cone, with each row located 38 mm from the last. These thermocouples have a response time on the order of a few microseconds[21] and have been successfully used for boundary layer transition determination in Adam and Hornung[4] and Rasheed et al.[8] The conical model geometry was chosen because of the wealth of experimental and numerical data available with which to compare the results from this program. Two photographs of the cone model are shown in Figure 1. The model is mounted such that the tip of the cone protrudes about 380 mm into the T5 nozzle at run time, in order to maximize the linear extent of the cone within the test rhombus defined by the expansion fan radiating from the nozzle's edge.

IV. Computational Model

In order to obtain the flow properties over the test cone, we start with the flow properties in the tunnel reservoir, which serves as the inflow for the nozzle flow simulations. The reservoir conditions are obtained by solving for chemical and thermal equilibrium at the specified reservoir pressure and enthalpy using the

Chemical Equilibrium with Applications (CEA) code. These conditions are allowed to expand through the nozzle using the CFD solver described below. For the current computational analysis, it is assumed that the boundary layer on the nozzle walls becomes turbulent in the reservoir and remains in this state for the remainder of the nozzle. A second CFD solver is used to simulate the flow over the test cone, also described below. The freestream properties over the cone are approximated by sampling the nozzle flow at the centerline of the nozzle exit and are held constant over the length of the cone. In the experiment, the freestream properties vary over the length of the cone due to the location of the cone in the nozzle. In all cases the wall temperature for the nozzle and cone walls is 297 K. Also for the computations, the cone nose has been approximated as sharp.

We simulate the flow through the nozzle by solving the reacting, axi-symmetric, two-dimensional Navier-Stokes equations with a structured-grid CFD solver as described in Candler[22] and Wagnild.[11] The solver uses an excluded-volume equation of state in order to properly capture the variation in gas properties at high pressure. The inviscid fluxes are calculated using the modified Steger-Warming flux vector splitting method and are second-order accurate with a MUSCL limiter as the TVD scheme. The viscous fluxes are second-order accurate. The time advancement method is the implicit, first-order DPLR method. The turbulent boundary layer flow is modeled using the one-equation, Spalart-Allmaras[23] model with the Catris-Aupoix[24] compressibility correction. The nozzle flow is calculated on a single-block, structured grid with dimensions 492 cells by 219 cells in the streamwise and wall-normal directions, respectively. The grid is clustered near the nozzle wall in order to sufficiently resolve the boundary layer.

Figure 1. Top: Aluminum cone, 1m in length, instrumented with 80 thermocouples in 20 rows. Bottom, from right to left: molybdenum tip, plastic holder with 316L stainless steel 10 micron porous section, aluminum cone body.

The mean flow for the stability analysis is calculated using a structured-grid, axi-symmetric CFD solver, which solves the reacting Navier-Stokes equations and is part of the STABL software suite.[25] This flow solver is also based on the finite-volume formulation and is similar to the one used to simulate the nozzle flow with the exception of the excluded volume equation of state. This specialized equation of state is not necessary for this solver because the static pressure over the cone is not sufficiently high to require an altered equation of state. The mean flow is computed on a single-block, structured grid with dimensions of 1001 cells by 301 cells in the streamwise and wall-normal directions, respectively. The wall-normal span of the grid increases down the length of the cone, from 4.1 mm at the tip to 23.5 cm at the base, allowing for the shock to be fully contained within the grid for all cases tested. The grid is clustered at the wall as well as at the nose in order to capture the gradients in these locations.

The stability analyses are performed using the PSE-Chem solver, which is also part of the STABL software suite. PSE-Chem[26] solves the reacting, two-dimensional, axi-symmetric, linear parabolized stability equations to predict the amplification of disturbances as they interact with the boundary layer. The PSE-Chem solver includes finite-rate chemistry and translational-vibrational energy exchange. The parabolized stability equations predict the amplification of disturbances as they interact with the boundary layer. The transition location is then predicted using the semi-empirical e^N approach, in which transition is assumed to occur when a disturbance has grown by a factor of e^N from its initial amplitude. The critical value of N is emperical and depends, among other factors, on the disturbance environment; therefore, N must be calibrated for a particular wind tunnel facility. Conventional, non-quiet, supersonic wind tunnels have been generally understood to have a transition N factor in the range of 5–6.[27] Both the mean flow and stability analysis solvers in STABL are capable of selectively freezing both chemical reactions and molecular vibration, allowing for the determination of internal molecular effects on boundary layer disturbances.

A seven-species chemistry model including CO_2, CO, N_2, O_2, NO, N, O is used to approximate the flow through the nozzle as well as over the cone for all conditions tested. In all computations, a finite-rate chemical reaction model is used, with reaction rates based on Park[28] and Bose and Candler.[29,30] The

equilibrium coefficients are calculated from fits based on Park[31] and McBride et al.[32] It is assumed that the vibrational-vibrational energy exchanges occur on a relatively short time scale, allowing for a single temperature governing all vibrational modes. It is also assumed that rotation and translation are coupled and governed by the translational temperature. The translational-vibrational energy exchanges are governed by the Landau-Teller model for the simple harmonic oscillator. The vibrational relaxation times are governed by the Millikan and White model with several empirical corrections given in Camac[18] and Park.[28] The viscosity for each species is calculated using Blottner fits and the mixture quantities are calculated using Wilke's semi-empirical mixing law.

V. Computational Predictions

Using the methods described above, seven test gas mixtures are simulated, each at four different freestream conditions. The gas mixtures are given based on the mass fraction of carbon dioxide in the mixture and are 0.0, 0.1, 0.2, 0.3, 0.5, 0.75, 1.0. The freestream conditions are chosen based on the reservoir pressure and the reservoir enthalpy and are 10 MJ/kg and 50 MPa, 8.5 MJ/kg and 45 MPa, 7 MJ/kg and 40 MPa, and 5 MJ/kg and 30 MPa. For each gas mixture, the formation enthalpy of the mixture is omitted from the reservoir enthalpy in order to make a proper comparison between test cases. To determine the predicted transition location on the test cone, a transition N factor of 5 is chosen. The transition locations along the cone surface are extracted from the results of the stability analyses of each case and are compiled in Figure 2. One objective of the current computations is to determine the regime in which a transition delay can be obtained. The data in Figure 2 show that an increase of the mass fraction of carbon dioxide in the 5 MJ/kg case has only a small effect on the transition location. At 7 MJ/kg, the transition location moves toward the rear of the cone by about 5 cm at 100% CO_2. The 8.5 MJ/kg case shows a shift in transition of approximately 61 cm. The 10 MJ/kg case results in the largest shift in the transition location, approximately 66 cm at 100% CO_2, indicating that carbon dioxide has a large potential for transition delay in this enthalpy range.

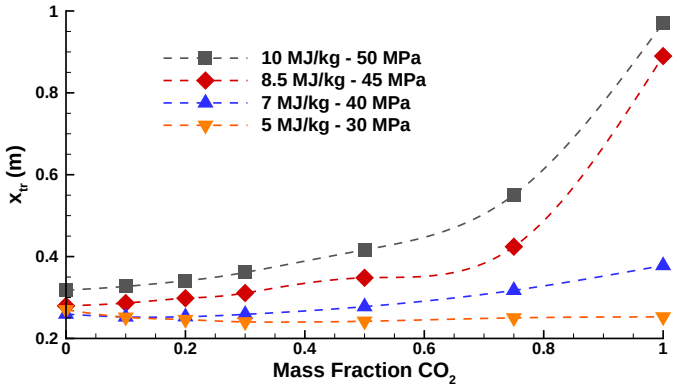

Figure 2. Comparison of the transition location based on a critical N factor of 5 versus mass fraction of CO_2 for each of the four freestream conditions.

In order to damp acoustic vibrations within the boundary layer, energy must be transferred into the gas molecules' internal modes, the energy content of which depends upon vibrational specific heat. Vincenti and Kruger[33] present Equation (3) for vibrational specific heat, where Θ_i is the characteristic vibrational temperature of each mode of the gas molecule, and R is the gas molecule's gas constant. The exponential factors dominate the vibrational contribution from each mode, and indicate that an increase in temperature causes an increase in both total specific heat and the contribution to specific heat from each vibrational mode.

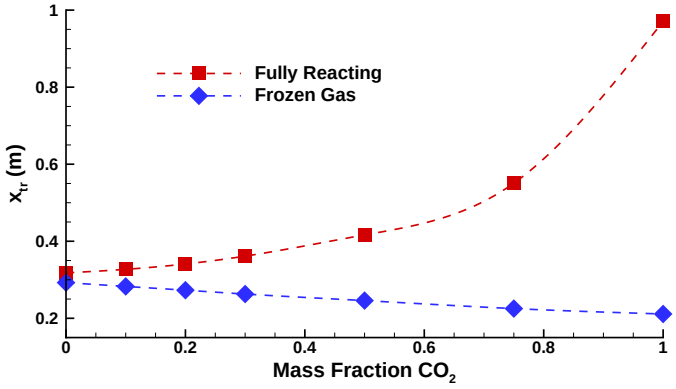

Figure 3. A comparison of the transition location versus mass fraction of CO_2 based on a N factor of 5 between a fully reacting and a frozen gas stability analysis at 10 MJ/kg and 50 MPa.

Specifically, as Θ_i/T becomes large (for small T), the summand tends to zero, which means there is no contribution to the vibrational specific heat from that vibrational mode. As Θ_i/T becomes small (for large T), the summand

tends to unity, and the maximum contribution from a given vibrational mode is therefore R. As temperature increases within the boundary layer, each mode becomes more fully excited and capable of exchanging more energy from acoustic vibrations. Temperature tends to increase with enthalpy. Table 1 on page 8 records reservoir enthalpy and T^*, a characteristic boundary layer reference temperature, for each experiment.

$$C_{v_{vib}} = R \sum_i \left\{ \left(\frac{\Theta_i}{T} \right)^2 \frac{e^{\Theta_i/T}}{\left(e^{\Theta_i/T} - 1 \right)^2} \right\} \tag{3}$$

Using the ability of the stability analysis in STABL to freeze the chemical and vibrational rate processes, we can determine the effect of these rate processes on the damping of second mode disturbances. An example of this type of calculation is demonstrated by comparing the transition location for a fully reacting stability analysis and a frozen gas stability analysis for the 10 MJ/kg case, as shown in Figure 3. Using a reacting mean flow and a frozen gas stability analysis, the data show that adding carbon dioxide promotes transition. When the chemical and vibrational rate processes are included in the stability analysis, the transition location moves further down the cone due to carbon dioxide's ability to damp boundary layer disturbances. By calculating the change in transition location, we can compare the effectiveness of disturbance damping in each of the four freestream conditions, shown in Figure 4. For all cases tested, the addition of chemical and vibrational rate processes results in a shift in the transition location towards the rear of the cone that increases with an increasing mass fraction of carbon dioxide in the test gas. From these data, it becomes clear that the damping ability of carbon dioxide is most effective for the 10 MJ/kg case, for the reasons described above. Interestingly, the addition of carbon dioxide in the 5 MJ/kg case has little or no effect as indicated in Figure 2, despite the disturbance damping ability of molecular vibration demonstrated in Figure 4. In this case, the optimum disturbance damping frequency of carbon dioxide is no longer similar to the boundary layer disturbance frequencies.

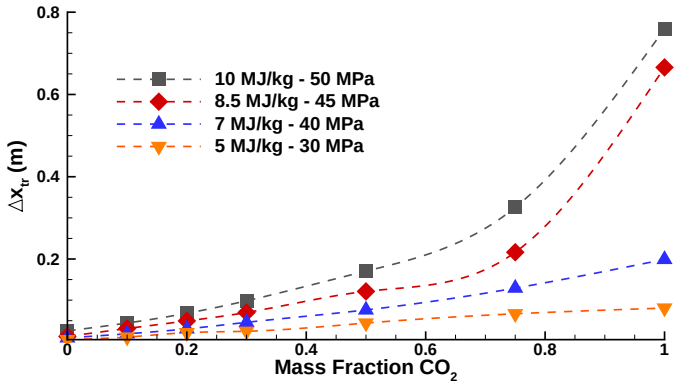

Figure 4. Comparsion of the change in transition location due to vibrational relaxation versus mass fraction of CO_2 based on a transition N factor of 5 for each of the three freestream conditions tested.

It is also noted that the relatively small effect of vibrational damping shown in Wagnild et al.[34] is due to the total enthalpy of the flow considered in their study, approximately 4.5 MJ/kg. As demonstrated in Figure 4, the vibrational damping of carbon dioxide causes a smaller change in transition location with a decreasing flow enthalpy. Thus, a small change in amplification at 4.5 MJ/kg is expected.

VI. Experimental Results

Although there have been several previous experimental campaigns on transition in T5 (Germain,[3] Adam and Hornung,[4] Leyva et al.,[9] Jewell et al.[12]), based on recent experience with T5 operations, it is desirable to conduct new experiments with special attention paid to repeatability and cleanliness of the tunnel. Based on the computations described above, we choose three carbon dioxide/air gas mixtures which were tested in T5 on the 5-degree half-angle cone, with reservoir enthalpies varying from 7.68–9.65 MJ/kg and reservoir pressures held as consistently as possible near 58 MPa, but varying from 53.4–60.7 MPa, to attempt to reproduce the largest shift in transition location implied by the computations. The gas mixtures, by mass fraction of carbon dioxide in the mixture, are 0.0 (e.g. all air), 0.5, 1.0. A summary of run conditions and results is presented in Table 1 on page 8. For the 0.5 mass fraction case, the CO_2 and air are not premixed.

The shock tube is filled sequentially and the gases allowed to diffuse into each other for approximately 15 minutes before each experiment.

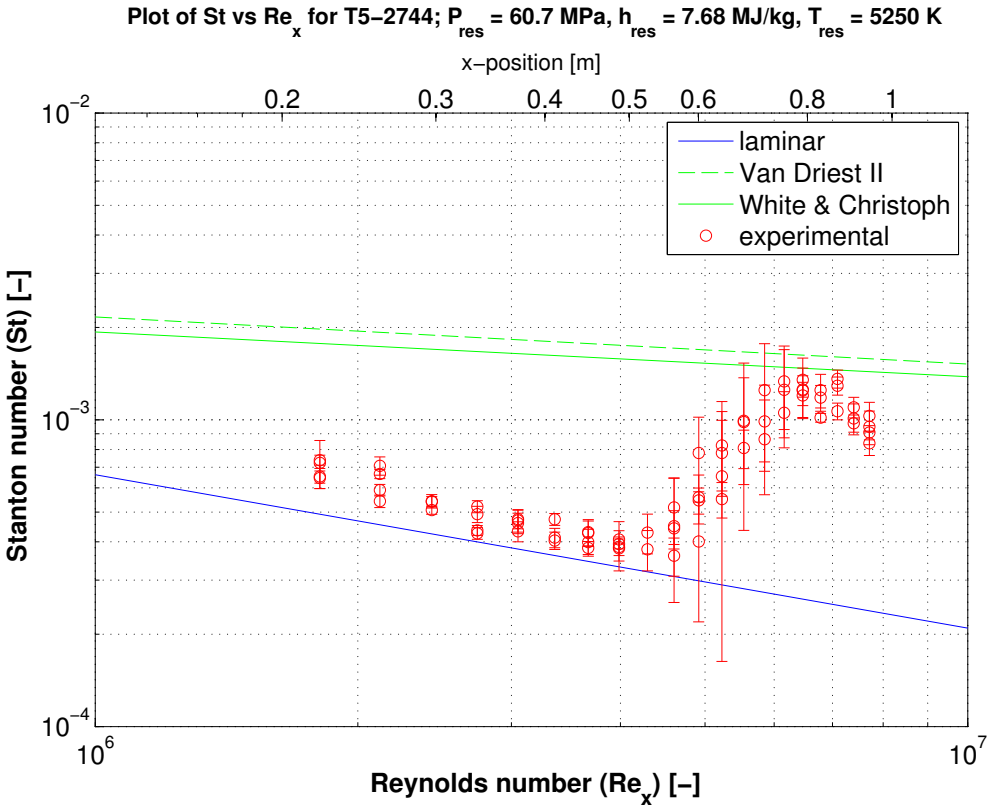

Figure 5. Time-averaged non-dimensional plot of heat transfer results in terms of Stanton number vs. Reynolds number for T5 shot 2744 in 100% air, with the laminar similarity correlation indicated in blue and two common turbulent correlations in green. The bars on each point represent the RMS values of each thermocouple's signal, and transition onset occurs at Re = 4.14×10^6, which is 0.505 m from the tip of the cone.

One example of results from the present tests, shot 2744 in air, is shown in Figure 5. Normalized heat-transfer results at 7.68 MJ/kg and 60.7 MPa are presented. The circles are time-averaged measurements from each of 80 thermocouples for the ∼1ms steady flow time, and the bars represent the root mean squared values from each sensor. The RMS bars are initially small in the laminar zone as the heat transfer levels are consistently at the laminar value, increase in size in the transitional zone as the flow becomes intermittent, and may then decrease in size again as the flow approaches the fully turbulent zone and heat transfer levels are consistently near the turbulent value. A slight drop-off from the fully turbulent value is observed in the last two rows of thermocouples, as they are positioned near the maximum extent of the T5 test rhombus and may intersect with the expansion fan emanating from the lip of the nozzle. For this experiment, transition is observed at 0.505 m from the tip of the cone.

Flow conditions in T5 are calculated from three tunnel measurements: the shock speed, initial shock tube fill pressure and composition, and reservoir pressure at the end of the shock tube during the run time. Shock speed is measured by two time of arrival pressure transducers positioned 2.402m apart, with an approximate measurement uncertainty of 8×10^{-6} s. The uncertainty in the shock speed measurement thus increases as the measured time of arrival difference decreases. At a shock speed of 3000 m/s, typical for the present study, the uncertainty is 30 m/s. The shock tube fill pressure uncertainty is 0.25 kPa, and the measured reservoir pressure uncertainty is typically 4 MPa. Uncertainties on the calculated quantities, including those represented by the error bars in Figures 6-8, are estimated by perturbing Cantera[35] condition computations[36] within the range of the uncertainties on the measured shock speed, reservoir pressure, and initial shock tube pressure. Only experiments with measured shock speeds that reasonably matched the adjusted shock speed curve predicted by the shock jump conditions from the burst pressure and initial conditions were included in the present data set.

Transition x-locations over the range of enthalpies for each gas mixture are summarized in Figure 6. A

Table 1. Run conditions and results included in the present study. In the last three columns, the > symbol indicates that the flow was laminar to the last measurable thermocouple location, which is recorded.

Experiment	w_{CO_2} (-)	h_{res} (MJ/kg)	P_{res} (MPa)	$T*$ (K)	x_{tr} (m)	Re_{tr} (-)	N_{tr} (-) †
2720	1	9.65	59.3	1845	> 0.824	$> 5.31 \times 10^6$	> 4.63
2729	0.5	8.45	57.7	1688	0.721	5.01×10^6	9.24
2730	0.5	7.80	58.1	1593	0.639	4.90×10^6	9.48
2732	0.5	7.84	57.0	1592	0.714	5.25×10^6	
2739	0	8.03	57.5	1618	0.547	3.98×10^6	
2740	0	7.97	57.3	1608	0.544	3.96×10^6	
2741	0	8.34	56.9	1665	0.567	3.89×10^6	10.57
2742	0	8.64	55.7	1719	0.581	3.80×10^6	
2743	0	9.09	56.3	1789	0.639	3.94×10^6	10.58
2744	0	7.68	60.7	1565	0.505	4.14×10^6	10.99
2745	1	9.67	58.5	1837	> 0.797	$> 5.00 \times 10^6$	
2747	1	9.36	60.3	1803	> 0.855	$> 5.75 \times 10^6$	> 5.02
2749	0.5	9.59	60.4	1860	> 0.829	$> 5.19 \times 10^6$	> 8.93
2750	0.5	9.00	60.0	1776	> 0.829	$> 5.58 \times 10^6$	> 9.57
2751	1	9.04	60.2	1756	> 0.835	$> 5.75 \times 10^6$	
2754	1	9.41	53.4	1799	> 0.805	$> 4.90 \times 10^6$	
2756	1	8.72	57.5	1710	> 0.821	$> 5.62 \times 10^6$	> 5.57

† N factor was not calculated for every experiment.

strong correlation between reservoir enthalpy and transition location is apparent for all gas mixtures, and delays of up to 30% (at 9.2 MJ/kg) are observed for flows containing CO_2 compared to experiments in pure air.

Figure 7 presents the same data in terms of the Reynolds number evaluated at boundary layer edge conditions, defined in Equation (4). Edge conditions are calculated from the conditions at the nozzle exit by iteratively solving the Taylor-Maccoll equation for a conical shock.

$$\mathrm{Re}_{tr} = \frac{\rho_e u_e x_{tr}}{\mu_e} \tag{4}$$

While experiments with CO_2 in the freestream remain distinct from air tests, this approach results in similar transition Reynolds numbers within each gas mixture condition, weakening the trend with reservoir enthalpy seen in the x-location data in Figure 6. In terms of Re, delays up to 38% (at ∼9.2 MJ/kg) are observed for the measured transition location in flows containing CO_2 compared to experiments in pure air.

Within a hypervelocity boundary layer, strong temperature gradients between the wall and the freestream result in strong gradients in fluid properties. To define a single representative Reynolds number, it is convenient to choose a single so-called reference temperature at which to evaluate density and viscosity. Experiments by Adam[4] showed that computing the transition Reynolds number at reference conditions strongly separated pure CO_2 results from pure air and N_2 data. The Dorrance[37] reference temperature, defined in Equation (5) has the same form as the Eckert reference temperature but may be used for other gases as well as air.

$$\frac{T^*}{T_e} = \frac{1}{2} + \frac{\gamma - 1}{2}\frac{\sqrt{\mathrm{Pr}}}{6}M_e^2 + \frac{1}{2}\frac{T_w}{T_e} \tag{5}$$

The Dorrance temperature is used to calculate the quantites in Equation (6), the Reynolds number with density and viscosity evaluated at reference conditions.

$$\mathrm{Re}^*_{tr} = \frac{\rho^* u_e x_{tr}}{\mu^*} \tag{6}$$

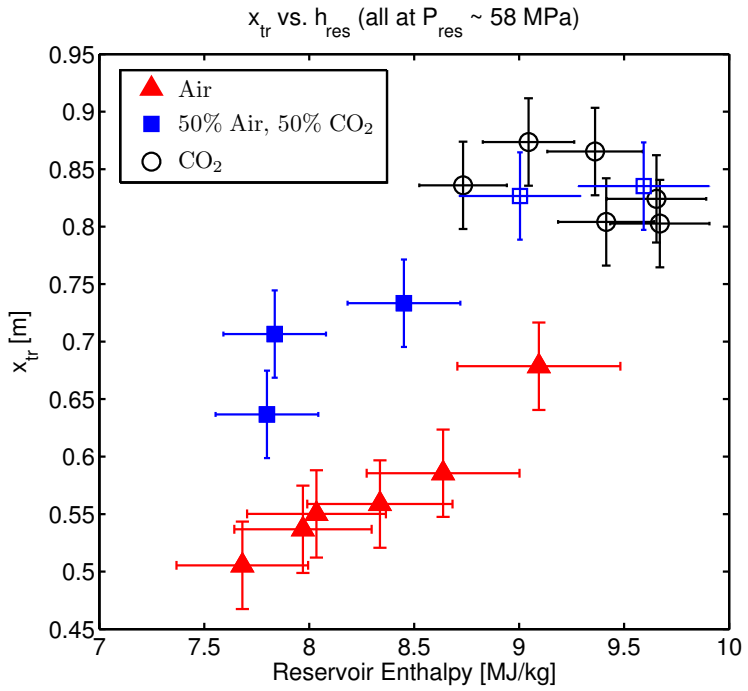

Figure 6. Location of transition on the cone surface vs. reservoir enthalpy, with reservoir pressure held near 58 MPa for all experiments. Solid symbols represent experiments which showed transition at the location indicated; hollow symbols represent experiments where no transition was observed, and are placed at the location of the last measurable thermocouple for that test.

The results of the present study calculated in terms of Re* are given in Figure 8. This approach effectively correlates observed transition locations for each gas mixture across the entire range of enthalpies examined, clearly separating air, CO_2 and mixture cases. In terms of Re*, delays up to 140% (at ~9.2 MJ/kg) are observed for the measured transition location in flows containing CO_2 compared to experiments in pure air. Using a similar cone in T5, and over a similar enthalpy range, Adam[38] reported values of Re^*_{tr} between 1.00×10^6 and 1.66×10^6 in pure air and between 5.40×10^6 and 8.06×10^6 in pure CO_2. The present air Re^*_{tr} values are significantly higher than Adam's air results, but the present CO_2 and air/CO_2 mixture results overlap with Adam's CO_2 results.

VII. Computational Analysis of Experiments

Using the computational method described above, several of the experimental cases are analyzed to determine the transition N factor. The results of several cases in this analysis are shown in Figure 9, which plots the maximum N factor reached along the length of the cone. The air shots are indicated with solid lines, the 50% CO_2 shots are indicated with dashed lines, and the 100% CO_2 shots are indicated with dot-dashed lines. For the conditions presented, it is apparent that the second mode amplification is decreasing with an increasing mass fraction of CO_2 as indicated by the magnitude of the N factor along the cone. The experimental transition locations of each shot are marked with hollow black diamonds on their corresponding maximum N factor curve.

The transition N factors for the 50% CO_2 cases lie below the air shots. However, both freestream compositions show transition near N~10. The calculated maximum disturbance amplification in the 100% CO_2 shots results in N<6, apparently insufficient to cause transition, although other factors may be important. The transition N factors of each shot where transition was observed are compiled in Figure 10 versus the reservoir enthalpy. The error bars on each datum indicate change in transition N factor due to a 4 cm uncertainty in the measurement of the transition location. It appears that in both the air and 50% CO_2 cases, an N factor of ~10 is appropriate for the prediction of transition location. However, as this is a purely empirical observation, we have no reason to expect that this should be the case for all mixtures and enthalpies. One potential reason for the slightly lower transition N factors in the 50% CO_2 shots may be that the stability analysis is overpredicting the damping ability of carbon dioxide. This could result from a

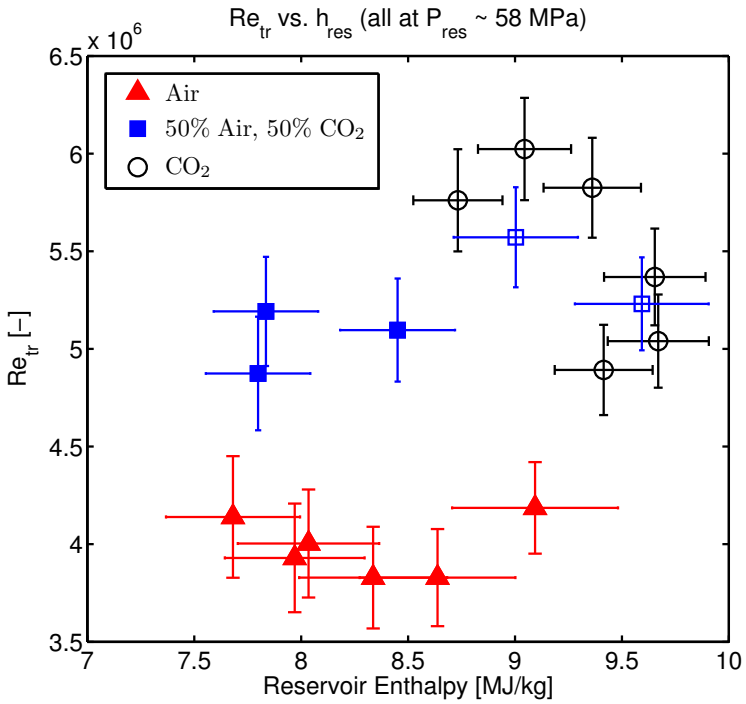

Figure 7. Reynolds number at transition (evaluated at edge conditions) vs. reservoir enthalpy, with reservoir pressure held near 58 MPa for all experiments. Solid symbols represent experiments which showed transition at the location indicated; hollow symbols represent experiments where no transition was observed, and are placed at the location of the last measurable thermocouple for that test.

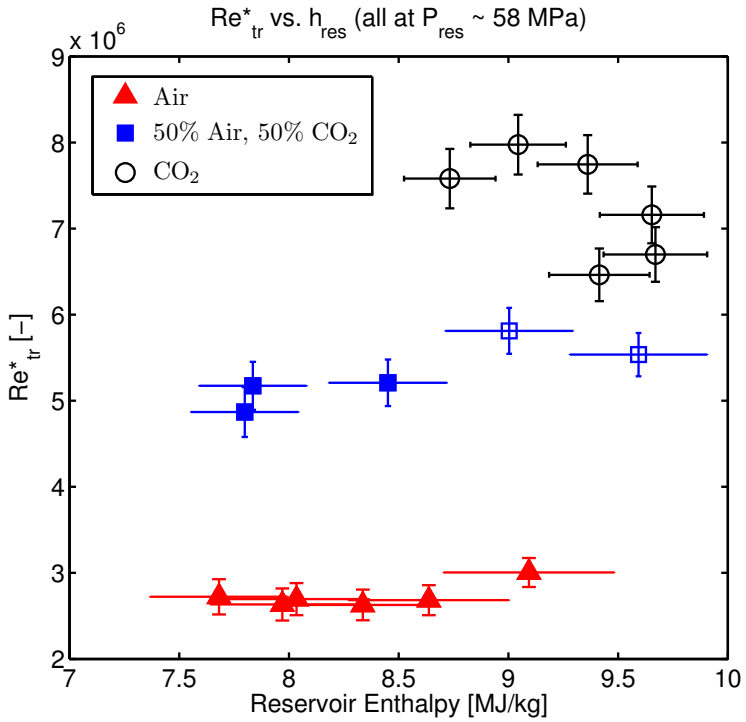

Figure 8. Reynolds number at transition (evaluated at Dorrance reference conditions) vs. reservoir enthalpy, with reservoir pressure held near 58 MPa for all experiments. Solid symbols represent experiments which showed transition at the location indicated; hollow symbols represent experiments where no transition was observed, and are placed at the location of the last measurable thermocouple for that test.

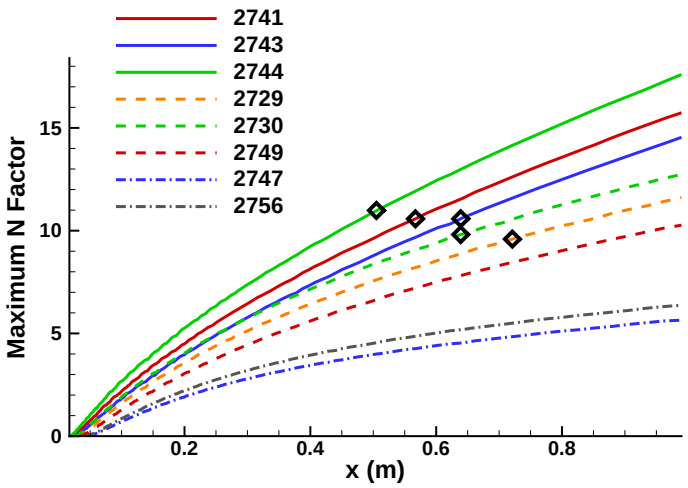

Figure 9. Maximum N factor vs. distance along the surface of the cone as computed by STABL for the conditions of the T5 shot indicated in the legend. The experimentally measured transition locations are indicated by hollow black diamonds where applicable. The solid lines (2741, 2743, 2744) are air cases, the dashed lines (2729, 2730, 2749) are 50% air, 50% CO_2 cases, and the dot-dashed lines (2747, 2756) are CO_2 cases.

different vibrational relaxation rate than that predicted by Camac's rates, or perhaps the simple harmonic oscillator model assumption is too idealistic for this experiment.

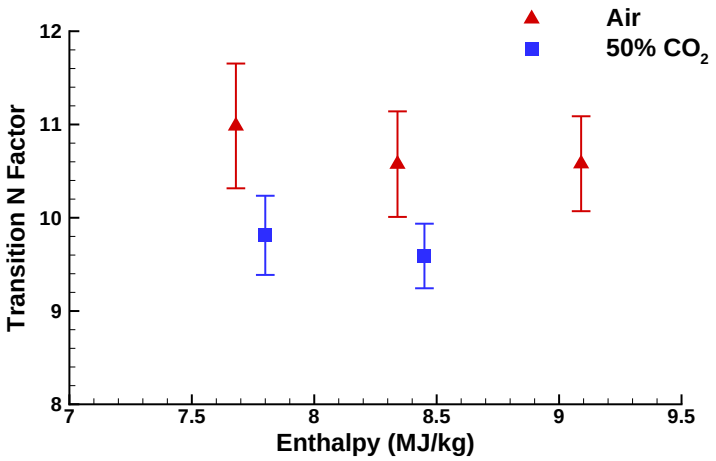

Figure 10. Transition N factor vs. reservoir enthalpy as computed by STABL for the experimental conditions at which transition was measured. The error bars represent the maximum change in N factor when varying the transition location by ± 4 cm.

The present experimental results are a closer match to the present computations than an earlier study,[5] which used a similar methodology with the assumption that transition occurred at an N factor of ~10, and found that transition Reynolds numbers were overpredicted by a factor of 2 when compared experimentally with T5 experiments performed by Adam.[4] These experimental and computational data also show more consistent behavior with varying conditions than an analysis performed by Wagnild.[11] Additionally, a computational analysis by Gronvall et al.[39] found a consistent transition N factor of approximately 8 for transition on a sharp 5-degree half-angle cone in the free-piston shock tunnel HIEST. Both Gronvall et al. and the current study indicate transition at higher levels of amplification than previous estimates for non-quiet tunnels. The current estimate of N~10 for T5 may be at least partially due to the suppression of particulate-induced transition through much more thorough cleaning of the compression tube, shock tube, nozzle, and other wetted components of T5 than has been standard practice in the past.

VIII. Conclusions and Future Work

Consistent transition N factors greater than 10 have been found over a 5-degree half-angle in the T5 hypervelocity shock tunnel for air flows with reservoir enthalpies above 7.68 MJ/kg and reservoir pressures near 58 MPa. N factors greater than 9 have been calculated for 50% air/CO_2 mixtures at equivalent enthalpy and pressure conditions. Transition location is an increasing function of both the reservoir enthalpy and CO_2 concentration. Addition of 50% CO_2 by mass results in an increase in transition distance of Re* by a factor of two, but the N factor is comparable in all cases, N∼9–11. This suggests that the suppression of the second mode through the absorption of energy from acoustic disturbances through vibrational relaxation is a mechanism for delaying transition both in high-enthalpy carbon dioxide flows and, more usefully, high-enthalpy flows consisting of a mixture of CO_2 and air.

These results are quite promising. Future work will include the installation of a premixing tank for studies using fully mixed CO_2 and air in the shock tube, to address concerns about completeness of the gaseous mixing process prior to each experiment; additional mass fraction cases; studies in gases other than CO_2; and ultimately continuation of the boundary-layer injection work begun in Jewell et al.[12]

Acknowledgments

The authors thank Mr. Nick Parziale for his assistance in running T5, Mr. Bahram Valiferdowsi for his work with design, fabrication, and maintenance, and Prof. Hans Hornung for his advice and support. The experimental portion of this project was sponsored by the Air Force Office of Scientific Research under award number FA9550-10-1-0491 and the NASA/AFOSR National Center for Hypersonic Research. The computational work was sponsored by the Air Force Office of Scientific Research grant FA9550-10-1-0352. Sandia National Laboratories is a multi-program laboratory managed and operated by Sandia Corporation, a wholly owned subsidiary of Lockheed Martin Corporation, for the U.S. Department of Energy's National Nuclear Security Administration under contract DE-AC04-94AL85000. The views expressed herein are those of the authors and should not be interpreted as necessarily representing the official policies or endorsements, either expressed or implied, of AFOSR, Sandia, or the U.S. Government.

References

[1]Mack, L. M., "Boundary-layer linear stability theory. special course on stability and transition of laminar flow advisory group for aerospace research and development," Tech. rep., 1984, AGARD Report No. 709.

[2]Malik, M. R., "Hypersonic flight transition data analysis using parabolized stability equations with chemistry effects," *Journal of Spacecraft and Rockets*, Vol. 40, No. 3, 2003, pp. 332–344.

[3]Germain, P., *The Boundary Layer on a Sharp Cone in High-Enthalphy Flow*, Ph.D. thesis, California Institute of Technology, Pasadena, CA, 1993.

[4]Adam, P. H. and Hornung, H. G., "Enthalpy effects on hypervelocity boundary-layer transition: Ground test and flight data," *Journal of Spacecrafts and Rockets*, Vol. 34, No. 5, 1997.

[5]Johnson, H. B., Seipp, T. G., and Candler, G. V., "Numerical study of hypersonic reacting boundary layer transition on cones," *Physics of Fluids*, Vol. 10, 1998, pp. 2676–2685.

[6]Fujii, K. and Hornung, H. G., "A Procedure to Estimate Absorption Rate of Sound Propagating Through High Temperature Gas," Tech. rep., California Institute of Technology, Pasadena, CA, Aug. 2001, GALCIT Report FM2001.004.

[7]Fedorov, A. V., Malmuth, N. D., and Hornung, H. G., "Stabilization of hypersonic boundary layers by porous coatings," *AIAA journal*, Vol. 39, No. 4, 2001, pp. 605–610.

[8]Rasheed, A., Hornung, H. G., Fedorov, A. V., and Malmuth, N. D., "Experiments on passive hypervelocity boundary-layer control using an ultrasonically absorptive surface," *AIAA Journal*, Vol. 40, No. 3, 2002, pp. 481–489.

[9]Leyva, I. A., Laurence, S., Beierholm, A. W., Hornung, H. G., Wagnild, R., and Candler, G., "Transition delay in hypervelocity boundary layers by means of CO2/acoustic instability interactions," *47th Aerospace Sciences Meeting*, AIAA, Orlando, FL, 2009, AIAA 2009-1287.

[10]Wagnild, R. M., Candler, G. V., Leyva, I. A., Jewell, J. S., and Hornung, H. G., "Carbon Dioxide Injection for Hypervelocity Boundary Layer Stability," *48th Aerospace Sciences Meeting*, AIAA, Orlando, FL, 2010, AIAA 2010-1244.

[11]Wagnild, R. M., *High Enthalpy Effects on Two Boundary Layer Disturbances in Supersonic and Hypersonic Flow*, Ph.D. thesis, University of Minnesota, Minneapolis, MN, 2012.

[12]Jewell, J. S., Leyva, I. A., Parziale, N. J., and Shepherd, J. E., "Effect of Gas Injection on Transition in Hypervelocity Boundary Layers," *Proceedings of the 28th International Symposium on Shockwaves*, Manchester, UK, 2011.

[13]Fedorov, A., "Transition and stability of high-speed boundary layers," *Annual Review of Fluid Mechanics*, Vol. 43, 2011, pp. 79–95.

[14]Stetson, K. F., "Hypersonic boundary-layer transition," *Advances in Hypersonics*, edited by J. Bertin, J. Periauz, and J. Ballman, Birkhauser, Boston, MA, 1992, pp. 324–417.

[15]Kinsler, L. E., Frey, A. R., Coppens, A. B., and Sanders, J. V., *Fundamentals of acoustics (Third Edition)*, John Wiley & Sons, Inc., New York, 1982.

[16]Clarke, J. F. and McChesney, M., *The dynamics of real gases*, Vol. 175, Butterworths, 1964.

[17]Zeldovich, Y. B. and Raizer, Y. P., *Physics of shock waves and high-temperature hydrodynamic phenomena*, Academic Press, New York, NY, 1967.

[18]Camac, M., "CO_2 relaxation processes in shock waves," *Fundamental Phenomena in Hypersonic Flow*, edited by J. Hall, Cornell University Press, 1966, pp. 195–215.

[19]Hornung, H., "Performance data of the new free-piston shock tunnel at GALCIT," *17th Aerospace Ground Testing Conference*, AIAA, Nashville, TN, 1992, AIAA 92-3943.

[20]Hornung, H. and Belanger, J., "Role and techniques of ground testing for simulation of flows up to orbital speed," *16th Aerodynamic Ground Testing Conference*, AIAA, Seattle, WA, 1990, AIAA 90-1377.

[21]Marineau, E. C. and Hornung, H. G., "Modeling and calibration of fast-response coaxial heat flux gages," *47th Aerospace Sciences Meeting*, AIAA, Orlando, FL, 2009, AIAA 2009-0737.

[22]Candler, G. ., "Hypersonic nozzle analysis using an excluded volume equation of state," AIAA 2005-5202.

[23]Spalart, P. R. and Allmaras, S. R., "A one-equation turbulence model for aerodynamic flows," *30th Aerospace Sciences Meeting and Exhibit*, AIAA, Reno, NV, 1992, AIAA 92-0439.

[24]Catris, S. and Aupoix, B., "Density corrections for turbulence models," *Aerospace Science and Technology*, Vol. 4, No. 1, 2000, pp. 1–11.

[25]Johnson, H. B., *Thermochemical Interactions in Hypersonic Boundary Layer Stability*, Ph.D. thesis, University of Minnesota, Minneapolis, MN, 2000.

[26]Johnson, H. B. and Candler, G. V., "Hypersonic boundary layer stability analysis using PSE-Chem," *35th Fluid Dynamics Conference and Exhibit*, AIAA, 2005, AIAA 2005-5023.

[27]Schneider, S. P., "Effects of high-speed tunnel noise on laminar-turbulent transition," *Journal of Spacecraft and Rockets*, Vol. 38, No. 3, 2001, pp. 323–333.

[28]Park, C., Howe, J. T., Jaffe, R. L., and Candler, G. V., "Review of Chemical-Kinetic Problems of Future NASA Missions, II: Mars Entries," *Journal of Thermophysics and Heat transfer*, Vol. 8, No. 1, 1994, pp. 9–23.

[29]Bose, D. and Candler, G. V., "Thermal Rate Constants of the $N_2 + O \rightarrow NO+ N$ Reaction Using Ab Initio $3A''$ and $3A'$ Potential Energy Surfaces," *Journal of Chemical Physics*, Vol. 104, No. 8, 1996, pp. 2825–2833.

[30]Bose, D. and Candler, G. V., "Thermal Rate Constants of the $O + N \rightarrow NO + O$ Reaction Based on the $2A'$ and $4A'$ Potential-Energy Surfaces," *Journal of Chemical Physics*, Vol. 107, No. 16, 1997, pp. 6136–6145.

[31]Park, C., *Nonequilibrium Hypersonic Aerothermodynamics*, Wiley, New York, 1990.

[32]McBride, B. J., Zehe, M. J., and Gordon, S., "NASA Glenn coefficients for calculating thermodynamic properties of individual species," Tech. rep., 2002, Report TP-2002-21155.

[33]Vincenti, W. G. and Kruger, C. H., *Introduction to Physical Gas Dynamics*, Wiley, New York, 1965.

[34]Wagnild, R. M., Candler, G. V., Subbareddy, P., and Johnson, H., "Vibrational Relaxation Effects on Acoustic Disturbances in a Hypersonic Boundary Layer over a Cone," *50th Aerospace Sciences Meeting*, AIAA, Nashville, TN, 2012, AIAA 2012-0922.

[35]Goodwin, D., "Cantera: An object-oriented software toolkit for chemical kinetics, thermodynamics, and transport processes," Available: http://code.google.com/p/cantera, 2009, Accessed: 12/12/2012.

[36]Browne, S., Ziegler, J., and Shepherd, J., "Numerical solution methods for shock and detonation jump conditions," Tech. rep., California Institute of Technology, Pasadena, CA, July 2008, GALCIT Report FM2006.006.

[37]Dorrance, W. H., *Viscous hypersonic flow: theory of reacting and hypersonic boundary layers*, McGraw-Hill, 1962.

[38]Adam, P. H., *Enthalpy Effects on Hypervelocity Boundary Layers*, Ph.D. thesis, California Institute of Technology, Pasadena, CA, 1997.

[39]Gronvall, J. E., Johnson, H. B., and Candler, G. V., "Boundary Layer Stability Analysis of the Free-Piston Shock Tunnel HIEST Transition Experiments," *48th Aerospace Sciences Meeting*, AIAA, Orlando, FL, 2010, AIAA 2010-0896.